

# Ultrafast Dynamics of Exciton Formation in Semiconductor Nanowires

Chaw Keong Yong, Hannah J. Joyce, James Lloyd-Hughes, Qiang Gao, Hark Hoe Tan, Chennupati Jagadish, Michael B. Johnston, and Laura M. Herz\*

*The dynamics of free electron–hole pairs and excitons in GaAs–AlGaAs–GaAs core–shell–skin nanowires is investigated using femtosecond transient photoluminescence spectroscopy at 10 K. Following nonresonant excitation, a bimolecular interconversion of the initially generated electron–hole plasma into an exciton population is observed. This conducting-to-insulating transition appears to occur gradually over electron–hole charge pair densities of  $2\text{--}4 \times 10^{16} \text{ cm}^{-3}$ . The smoothness of the Mott transition is attributed to the slow carrier-cooling during the bimolecular interconversion of free charge carriers into excitons and to the presence of chemical-potential fluctuations leading to inhomogeneous spectral characteristics. These results demonstrate that high-quality nanowires are model systems for investigating fundamental scientific effects in 1D heterostructures.*

## 1. Introduction

The successful incorporation of semiconductor nanowires (NWs) into opto-electronic and photovoltaic devices as both elements and interconnects has sparked intense interest in the nature of carrier dynamics in such nanoscale materials.<sup>[1–6]</sup> Optical probing of ultrafast carrier dynamics in these materials has provided valuable insights here into both the quantum-confined and surface-mediated behavior of carriers.<sup>[7–10]</sup> For nanowires with diameters much larger than the exciton Bohr radius, the carrier relaxation is strongly affected by

unsaturated surface defects, which also increase the nonradiative recombination rate of excitons.<sup>[11–13]</sup> We have previously shown that by overgrowing the NW surface with a layer of large-bandgap semiconductor, the surface defect density can be reduced tremendously resulting in strong increases of charge carrier lifetimes towards their intrinsic bulk values.<sup>[14]</sup>

The conducting-to-insulating phase transition in semiconductor has been studied extensively both in bulk and 2D structures<sup>[16–21]</sup> since the original concept was developed by Mott.<sup>[22]</sup> In a semiconductor, such transitions result from screening of the attractive Coulomb interaction between an electron and a hole by the surrounding bound or free charge pairs, which increases with pair density. Following nonresonant excitation, the photoluminescence (PL) of a semiconductor with direct bandgap is first characterised by the recombination of unbound electron–hole pairs with Fermi-energy that shows significant occupation at high energy and bandgap renormalization (BGR) caused by exchange and correlation effects. As the pair density reduces, excitonic emission subsequently begins to dominate the PL spectra. Despite initial expectations, Mott transitions have often been found to be smooth crossovers across a range of electron–hole pair densities for both bulk semiconductors<sup>[21,23]</sup> and 2D semiconductor quantum wells.<sup>[24,25]</sup>

We report here on femtosecond time-resolved measurements conducted to investigate the transition from an

C. K. Yong, Dr. H. J. Joyce, Dr. J. Lloyd-Hughes,  
Dr. M. B. Johnston, Prof. L. M. Herz

Department of Physics  
Clarendon Laboratory  
University of Oxford  
Parks Road, Oxford, OX1 3PU, UK  
E-mail: l.herz1@physics.ox.ac.uk

Dr. Q. Gao, Prof. H. H. Tan, Prof. C. Jagadish  
Department of Electronic Materials Engineering  
Research School of Physical Sciences and Engineering  
Institute of Advanced Studies  
Australian National University  
Canberra ACT 0200, Australia



DOI: 10.1002/sml.201200156

initial hot electron–hole plasma to a relaxed exciton density in high-quality GaAs–AlGaAs–GaAs core–shell–skin NWs at substrate temperatures of 10 K. The coaxial type-I hetero-junction confines all carriers within the GaAs core through the use of the higher bandgap AlGaAs shell layer. The resulting nearly defect-free NW core allows the observation of contributions to the photoemission from both free (uncorrelated) and bound charge pairs (excitons). We find that following nonresonant excitation with a femtosecond pulse, the NW emission reveals a fast, charge-density-dependent interconversion from the initial free electron–hole plasma to a predominant exciton population. We are able to quantify the time-evolution of this conducting-to-insulating transition through the use of a coupled rate equation model that accounts for the bimolecular formation of excitons from the plasma, exciton-carrier ionization and radiative recombination. In addition, we directly monitor the charge dynamics at the Mott transition from time-resolved PL spectra. We find that with time after excitation, the homogeneous line width of the emission reduces gradually, while the PL peak becomes centered at the exciton energy and bandgap renormalization effects are reduced below the exciton binding energy. All three markers indicate that the Mott transition in high-quality NWs occurs gradually with decreasing charge pair density around a range of  $2\text{--}4 \times 10^{16} \text{ cm}^{-3}$ . We suggest two possible reasons for the origin of the smooth transition, which are the long time taken for the carrier cooling to the lattice temperature during the bimolecular interconversion of free charge carriers into excitons and the presence of inhomogeneities that may lead to local chemical potential fluctuations in the NWs. We find that if the passivating shell layer is absent (i.e., in “bare” GaAs core NWs) both free-charge pair and exciton dynamics become dominated by rapid trapping at defect sites within a few picoseconds after excitation.

## 2. Results and Discussion

### 2.1. Time-Integrated PL Spectra from GaAs Nanowires

**Figure 1a** shows a scanning electron microscopy (SEM) image of the as-grown GaAs nanowires under investigation: these comprised a GaAs core of 50 nm diameter, overcoated with a 30 nm thick AlGaAs shell which was protected by an outer skin layer (5 nm of GaAs). As previously reported, GaAs core–shell–skin (CSS) nanowires exhibit low defect density<sup>[14]</sup> allowing the observation of strong photoluminescence following excitation. **Figure 1b** shows the normalized time-integrated PL spectra measured for these NWs for a range of excitation fluences. At low excitation fluence, the PL spectrum is dominated by free exciton recombination (sharp peak at 1.521 eV) and also displays a weaker defect-mediated exciton recombination (peak at 1.50 eV). These defect trapping sites saturate quickly and free-exciton recombination is found to dominate the PL spectrum for excitation fluences above  $\sim 0.2 \mu\text{J cm}^{-2}$ , indicating the high-quality nanowires obtained from such growth mechanism. As the excitation fluence is increased further, a high-energy tail begins to emerge above the exciton energy, which we

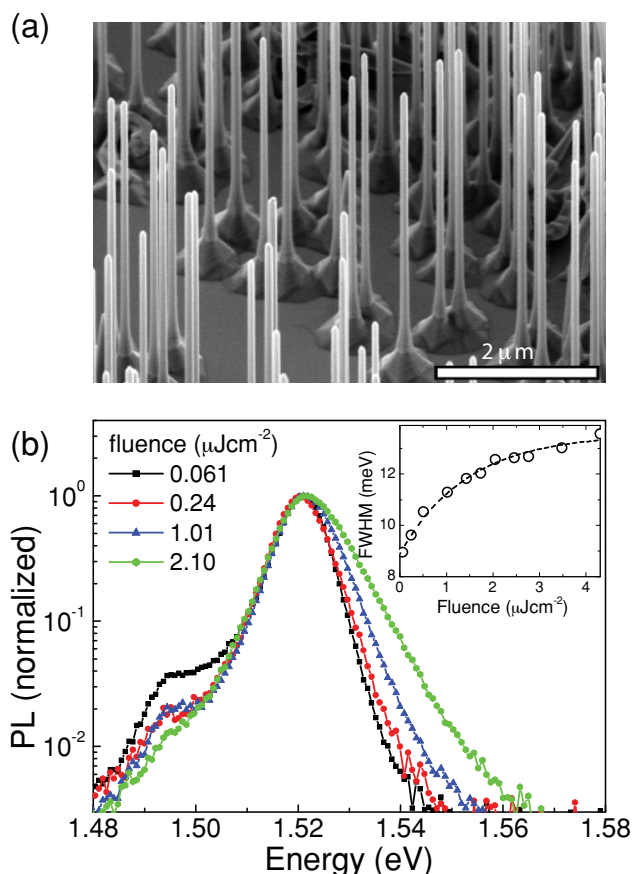


**Figure 1.** a) The SEM image of as-grown GaAs core–shell–skin nanowires on a GaAs(111)B surface. b) Normalized time-integrated PL spectra of GaAs core–shell–skin nanowires at 10 K for a range of excitation fluences. The inset shows the full-width at half-maximum (FWHM) of the full PL spectra as a function of excitation fluence. The dashed line is a guide to the eye.

ascribe to an increasing contribution of band-to-band plasma recombination to the emission. **Figure 1b** further reveals that the peak of the PL remains fixed at the exciton emission energy of the NWs while the intensity of the higher-energy electron–hole plasma emission increases successively with the excitation density. The inset of **Figure 1b** demonstrates a gradual increase of the full-width at half-maximum (FWHM) of the overall PL, as the excitation density is increased. These data therefore suggest that as the nonresonant excitation density is increased, the formation of excitons from initially created unbound free-carrier is weakened, which can be attributed to increasing charge-carrier screening effects.<sup>[20]</sup>

### 2.2 Time-Resolved Nanowire Emission and Analysis

In order to probe the dynamic exchange between such exciton and electron–hole plasma populations we conducted time-resolved PL measurements on the GaAs–CSS nanowires. We recorded the dynamics of the exciton population at the exciton emission peak ( $E_x = 1.52 \text{ eV}$ ) and monitored the electron–hole radiative plasma recombination at suitably

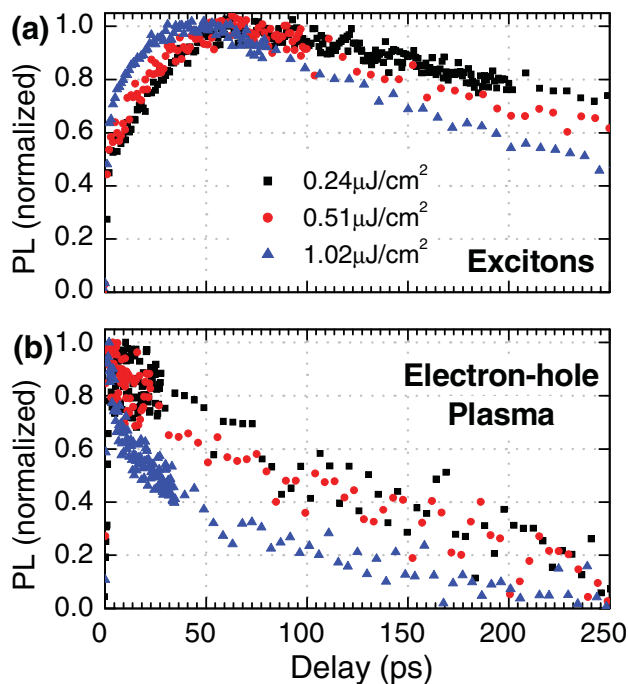


**Figure 2.** a) Normalized PL transients of GaAs-CSS NWs measured at the emission energy of the exciton at 1.52 eV for a range of excitation fluences. b) Normalized radiative plasma decay traces measured at 1.55 eV. The spectral window over which PL was collected is set by the system’s resolution (0.03 eV) which is limited by the high time resolution (200 fs).

higher energy ( $E_{\text{ch}} = 1.55$  eV) in order to avoid overlapping signals. In addition, we kept the excitation fluence range low ( $\leq 1 \mu\text{J cm}^{-2}$ ) in order to ensure that contaminating contributions from the plasma emission at the exciton emission energy were negligible.

**Figure 2** shows the normalized emission transients measured for exciton recombination and electron–hole plasma recombination. With increasing injected charge carrier density, the excitonic PL rises increasingly fast and decays increasingly quickly. This fast initial rise of the excitonic PL is matched by a corresponding decay of the electron–hole plasma recombination, both of which exhibit a fast ( $\sim 5$  ps) and a slow component ( $\sim 150$  ps). These dynamics suggest that excitons in high-quality NWs are formed via bimolecular recombination of the uncorrelated electron–hole plasma, which may be mediated by interaction of carriers with longitudinal optical (LO) and acoustic (AC) phonons.<sup>[28]</sup> Such mechanisms have previously been observed for 2D quantum wells:<sup>[29]</sup> with increasing carrier density, the increased probability of binding an electron to a hole through phonon interaction was found to lead to an increase in the exciton formation rate. Here we demonstrate that high-quality GaAs nanowires can also exhibit such slow, bimolecular exciton formation from an initially generated uncorrelated electron–hole plasma.

We may rule out alternative explanations for the observed dynamics, such as charge trapping or bimolecular exciton–exciton annihilation for the following reasons.

Charge carrier trapping, e.g., at surface defects, should lead to increasing excitonic emission lifetimes with increasing fluence near the trap saturation regime<sup>[14]</sup> or negligible fluence-dependence significantly below it, which is contrary to what we observe. Exciton–exciton annihilation processes are also unlikely to be of any influence here because in bulk semiconductors they are restricted by energy and momentum conservation requirements<sup>[30]</sup> and even in quantum wires, where such restrictions are lifted, these processes operate at charge densities that are over two orders of magnitude higher<sup>[30,31]</sup> than those employed here.

To gain further insight into the dynamics of exciton formation from free carriers, we apply a model based on coupled rate equations that includes carrier–exciton interconversion as well as radiative and nonradiative recombination of excitons and free carriers.<sup>[32]</sup> Here, the exciton formation constant  $C$  governs the bimolecular formation of excitons with density  $X$  from an electron–hole plasma with charge density  $n$ . Recombination within the uncorrelated electron–hole plasma is governed by both radiative, bimolecular mechanisms (plasma constant  $B$ ) or nonradiative, defect-mediated mechanisms ( $\tau_{\text{nr}}$ ) while exciton recombination is a monomolecular process with lifetime  $\tau_{\text{NW}}$ :

$$\begin{aligned} \frac{dn}{dt} &= -Cn^2 + Cn_{\text{eq}}^2 - \frac{n}{\tau_{\text{nr}}} - Bn^2, \quad n(0) = n_i; \\ \frac{dX}{dt} &= Cn^2 - Cn_{\text{eq}}^2 - \frac{X}{\tau_{\text{NW}}}, \quad X(0) = 0. \end{aligned} \quad (1)$$

where  $n_i$  is the injected carrier density. As shown by Piermarocchi et al.,  $C$  can be further divided into contributions arising from both acoustic ( $C_{\text{AC}}$ ) and optical ( $C_{\text{LO}}$ ) phonons, both of which mediate the exciton formation process<sup>[28]</sup> (see Supporting Information (SI) for more details). The recombination lifetime of excitons,  $\tau_{\text{NW}}$ , can be directly determined from the excitonic emission at long times after excitation, for which free-charge interconversion into excitons has been completed. For this purpose, we extended the measurements shown in Figure 2a to long (1.5 ns) delay times using a time-correlated single photon counting (TCSPC) system (see SI). The monoexponential decay of the excitonic PL at long delay time thus allows us to extract an exciton recombination lifetime of  $\tau_{\text{NW}} = 420$  ps from single-exponential fitting. Furthermore, the extracted exciton recombination rate is independent on the excitation density at the low excitation fluences used, which supports the notion of a low defect density in these high-quality nanowires. We therefore set the nonradiative free-charge recombination constant to a large value of  $\tau_{\text{nr}} = 1000$  ps, to reflect that such defect-mediated processes are unlikely to have any significant effect on the free-charge plasma decay. The radiative plasma recombination constant  $B$ <sup>[33]</sup> is taken to be the value for bulk GaAs,  $B \approx 6.9 \times 10^{-19} \text{ cm}^3 \text{ ps}^{-1}$ , given that the nanowires investigated here exhibit negligible quantum confinement. Finally,  $n_{\text{eq}}(n, X, T)$  is the equilibrium free carrier concentration given by the law of mass-action,<sup>[34,35]</sup> for which we again chose the 3D (bulk) version:<sup>[36]</sup>

$$\frac{n_{\text{eq}}^2}{X} = K(T_e) = 2 \left( \frac{\mu_X k_B T_e}{2\pi\hbar^2} \right)^{1.5} \exp\left(-\frac{E_B}{k_B T_e}\right), \quad (2)$$

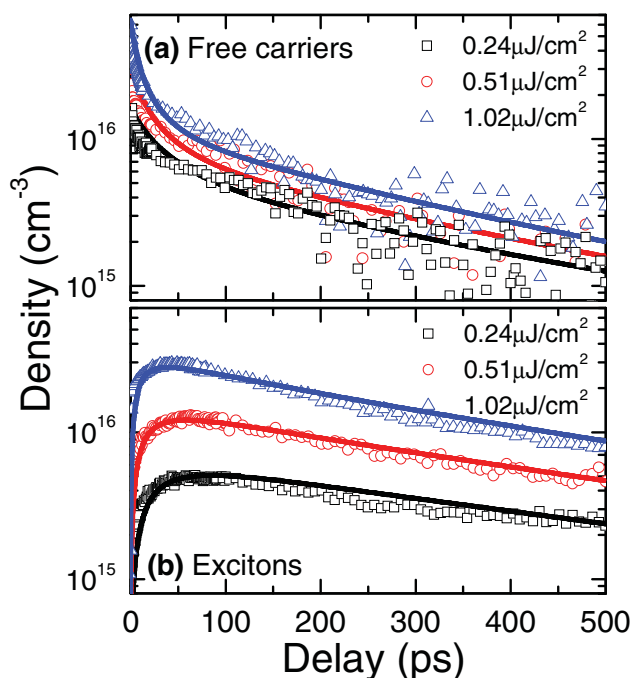


**Figure 3.** a) Free carrier density  $n$  and b) exciton density  $X$  in the GaAs-CSS NWs as a function of time after excitation for three different excitation fluences. Open symbols are data points while solid lines are fits based on the coupled-rate equation model described in the text. The experimental data for the free carrier density were converted from the decay traces of the radiative plasma emission shown in Figure 2b using the method described in the SI.

where  $\mu_x$  is the reduced exciton mass and  $E_B$  is the exciton binding energy (taken to be the GaAs bulk values of  $0.0546m_e$  and  $4.6 \text{ meV}$ ,<sup>[20]</sup> respectively) and  $K$  is the equilibrium constant which depends on the carrier temperature  $T_c$ . The term  $Cn_{\text{eq}}^2$  therefore describes the exciton ionization rate.<sup>[35]</sup>  $\hbar$  and  $k_B$  are the reduced Planck's constant and the Boltzman constant, respectively.

The photoluminescence data shown in Figure 2 directly link to the exciton density  $X$  and free carrier density  $n$  that are the solutions to Equation 1. First, the emission transients taken at the exciton emission energy (Figure 2a) are directly proportional to  $X(t)$ . Second, the free-charge density  $n(t)$  can be computed from the measured plasma emission  $I_{\text{plasma}}$  (Figure 2b) using their direct relationship,  $n \propto \sqrt{I_{\text{plasma}} T_c^{1.5}}$ . We use the well-established functions describing the charge carrier cooling processes in bulk GaAs<sup>[37]</sup> in order to extract  $n$  from  $I_{\text{plasma}}$  with the result shown in **Figure 3**. Details of the full procedure used for extracting  $n$  in this manner are provided in the SI.

Figure 3a,b show the best fits to the free-carrier and exciton densities data obtained through the solution of the coupled rate Equation 1, with  $C_{\text{AC}}$  and  $C_{\text{LO}}$  being the only free parameters. The excellent agreement between the data and the model confirms the occurrence of a gradual conducting-to-insulating transition in the nanowires, i.e., excitons are formed over time through a bimolecular process from unbound free carriers. The faster decay of excitonic PL at higher excitation density is therefore attributable to the faster

exciton generation. Here, the contribution of band-to-band recombination of unbound free-charge-carrier becomes dominant at increasing excitation density and competes directly with the exciton formation at early time delay. The transition from a conducting to an insulating phase occurs at later times after excitation, as a result of the decreasing screening efficiency of charge-carriers in the nanowires.<sup>[16,17]</sup>

We have also carried out identical measurements on GaAs nanowires that lack the shell-passivating layers of AlGaAs and GaAs. For these “bare” GaAs nanowires we find that both excitonic and charge carrier recombination is dominated by the rapid trapping at surface defects (see SI) in agreement with previous measurements of time-resolved terahertz conductivity dynamics in these materials.<sup>[13,14]</sup> By again fitting model solutions to the data as described above and using identical parameters, but letting  $\tau_{\text{NW}}$  and  $\tau_{\text{nr}}$  vary, we extract a value of 6 ps for these two time constants. These results show that effective defect passivation must be achieved in order for semiconductor nanowires to display intrinsic excitonic and charge properties.

### 2.3 Spectral Evolution of the Nanowire Emission

To gain further insights into the conducting-to-insulating transition, we measured the time-evolution of the PL spectra for GaAs-CSS nanowires under different excitation fluences. Two representative sets of time-resolved PL spectra measured at excitation fluences of 0.5 and  $1 \mu\text{J cm}^{-2}$  are shown in **Figure 4**. At early time delay, the PL is blue-shifted from the exciton energy and spectral broadening can be observed, with Fermi-filling<sup>[21,25]</sup> causing charge recombination above the band edge. At longer time-delay, the PL spectra shift to the centre at the exciton peak energy and spectrally narrow. These changes occur as the free-carrier density is depleted by band-to-band recombination and exciton formation until a predominantly excitonic phase has formed.<sup>[8,21]</sup>

For a more quantitative analysis, **Figure 5** plots the peak position of the PL spectra as a function of time, together with the total electron-hole pair density ( $N = n + X$ ) extracted from the model as described above. For PL spectra collected under initial excitation fluence of  $0.5 \mu\text{J cm}^{-2}$ , the PL peak centers at the exciton emission energy at a time delay of  $\sim 30$  ps. This occurs at longer time delay of  $\sim 150$  ps, when the excitation fluence is increased to  $1 \mu\text{J cm}^{-2}$ . These observations confirm that an increasing contribution to the total PL comes from the radiative recombination of free charge carriers as the fluence is increased, consistent with the time-integrated PL measurements shown in Figure 1. In theoretical support of this argument, we calculate the bandgap renormalization energy (BGR), as induced by the exchange and correlation of electron-hole pairs in the nanowires. It has been established that an excitonic phase appears when the BGR is comparable to the excitonic binding energy ( $E_B$ ). Vashishta and Kalia<sup>[38]</sup> showed that the sum of the exchange and correlation energies is independent of the band structure and can be determined from the electron-hole pair density and exciton binding energy as:

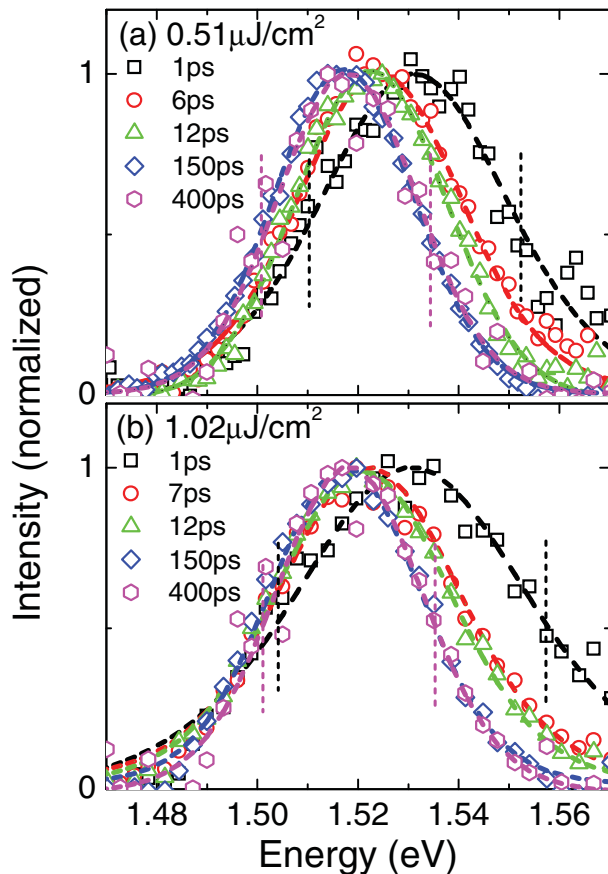


**Figure 4.** PL spectra obtained at various times after pulsed excitation with fluences of a) 0.51 and b) 1.02  $\mu\text{J cm}^{-2}$  for GaAs-CSS NWs. At early times, both high-energy emission from the electron–hole plasma and excitonic emission are observable, while at late times the PL converges towards predominantly excitonic emission. The pairs of vertical dashed lines indicate the spectral linewidths at half maximum for early (1 ps) and late (400 ps) time-delays. At later times after excitation, the predominantly excitonic spectra are broadened by both the spectral resolution of the system (limited by the high time resolution) and nanowire inhomogeneities.

$$\Delta_{\text{BGR}} = \frac{-E_{\text{B}}(-4.8316 - 5.0879r_s)}{0.0152 + 3.0426r_s + r_s^2}, \quad (3)$$

where  $r_s$  is a dimensionless quantity defined by the volume occupied by a carrier pair in the plasma compared with that for an exciton of radius  $a_b$ , that is,  $r_s = (4/3n\pi a_b^3)^{-1/3}$ . By taking the uncorrelated plasma density  $n$  from the fits to the emission transients as described above, we are able to plot the theoretically expected value ( $E_{\text{eh}} + \Delta_{\text{BGR}}$ ) of the low-energy emission edge (red line) in Figure 5, together with the overall electron–hole pair density  $N = n + X$  (blue line) and PL peak position (green diamonds). We find that the PL peak gradually shifts to become centered at the exciton emission energy, simultaneously with the band edge  $E_{\text{eh}} + \Delta_{\text{BGR}}$  (red line) crossing the exciton line (dashed black line). At this point the Coulomb screening becomes effectively weaker than the exciton binding<sup>[20]</sup> which therefore marks the commencement of the excitonic phase. This transition appears to be smooth and gradual and occurs when the total electron–hole pair density is reduced to  $\sim 2\text{--}4 \times 10^{16} \text{ cm}^{-3}$ . These data

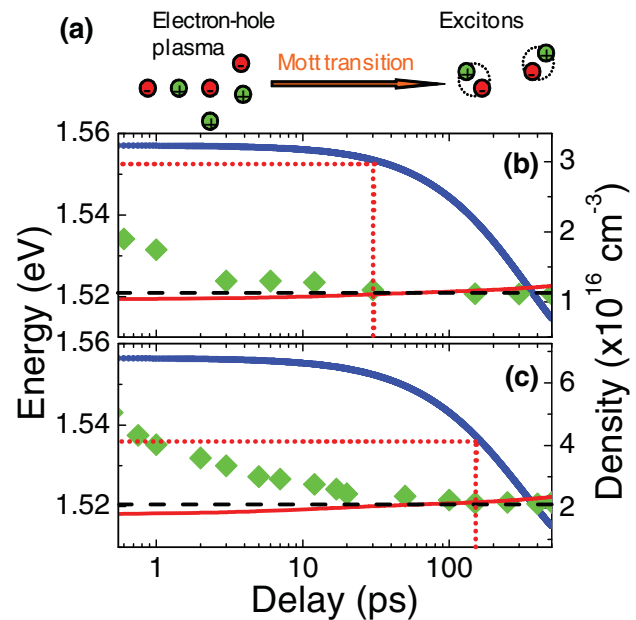


**Figure 5.** a) Schematic diagram for the Mott transition from uncorrelated free charge carriers into excitons. Temporal evolution of the peak energy of the total emission spectrum including plasma and excitonic contributions (green diamond) and the calculated band edge position (red solid line) and total electron–hole pair density (blue solid line) for excitation fluences of b) 0.51 and c) 1.02  $\mu\text{J cm}^{-2}$ . The exciton emission energy is indicated as dashed black line while the dotted red lines are a guide to the eye indicating where the Mott-transition commences.

also show again that as the excitation density is increased, the free-carrier-to-exciton interconversion is weakened by the presence of Coulomb screening, resulting in delayed commencement of the excitonic phase and enhanced carrier recombination via direct band-to-band transitions. These observations therefore support the model described above and are consistent with the time-integrated emission spectra shown in Figure 1b.

Such smooth transitions from an excitonic to a free charge plasma phase have been found previously to occur for both bulk semiconductors<sup>[23]</sup> and quantum wells.<sup>[25,32]</sup> We give two main reasons for why a gradual transition may also be observed for the GaAs nanowires investigated here. First, it is well-established that the carrier cooling is rather slow in GaAs due to the weak acoustic phonon coupling<sup>[37]</sup> and hence the carrier temperature  $T_c$  is higher than the lattice temperature  $T_l$  over the 500 ps observation window (see SI). The Mott criterion depends on the charge carrier temperature (for thermal lattice energies smaller than the exciton binding energy)<sup>[20]</sup> and therefore evolves with time after nonresonant excitation. In particular, the bimolecular interconversion of free charge carriers into excitons in the nanowires occurs concomitantly with the slow carrier cooling which can induce a broadening of the observed transition from an electron–hole plasma to an excitonic phase. The Mott density  $N_M$  denotes the electron–hole pair density at which the Debye–Hückel screening length ( $K_D$ ) becomes comparable to the exciton Bohr radius ( $a_b$ ), which yields:<sup>[20]</sup>

$$N_M = (1.19^2) \frac{\epsilon_r \epsilon_0 k_B T_e}{e^2 a_b^2} \quad (4)$$

where  $\epsilon_0$  is the vacuum permittivity and  $\epsilon_r$  is the relative dielectric constant. In a bulk semiconductor, excitons are expected to become unstable when the electron–hole pair density exceeds the Mott limit. We calculated the theoretical Mott density from Equation 4 using the simulated carrier temperature (see SI) and find that following initial fast carrier cooling within the first 10 ps after excitation,  $N_M$  decreases from  $\sim 4 \times 10^{16}$  to  $2 \times 10^{16} \text{ cm}^{-3}$  over the next 500 ps. These values are in excellent agreement with those we observe from the experimental spectral features shown in Figure 5. At excitation fluences significantly higher than those employed in these transient PL measurements, the Mott limit will be exceeded and we indeed observe a distinct quenching of the excitonic emission and increase in plasma contribution to the time-integrated PL spectra for excitation fluences exceeding  $\sim 1.5 \mu\text{J cm}^{-2}$  (see Figure 1b).

A second plausible cause for the observed gradual Mott transition is the existence of inhomogeneities in the material. We may rule out the presence of charge carrier density gradients in the nanowires as our experimental conditions were carefully chosen to avoid these (see SI). However, the TIPL spectra of the nanowires show an exciton linewidth that is much larger than thermal broadening effects to be expected at 10 K. This suggests that carriers within the nanowires experience chemical potential fluctuations which may also affect their confinement and Coulomb interaction energies, leading to partially overlapping emission features from excitons and free-carriers. Such variations can possibly arise from composition gradients, nanowire diameter fluctuation or unexpected doping near the core–shell interfaces during the growth. Previous measurements on single GaAs nanowires produced from similar growth techniques have shown linewidth broadening of 23 meV at 10 K, attributed to strain and compositional non-uniformities.<sup>[15]</sup> It should be stressed that the measurements presented here were carried out on nanowire ensembles and hence further broadening is to be expected. SEM images show that both nanowire-to-nanowire diameter changes ( $\pm 5 \text{ nm}$ ) and slight ( $< 3 \text{ nm per micrometer length}$ ) tapering of individual nanowires<sup>[26]</sup> occur in these materials. Variations in lateral width are common features even in high-quality semiconductor nanostructures and have been investigated in detail for 2D heterostructures<sup>[40]</sup> and more recently for tetrapod nanostructures.<sup>[41]</sup>

### 3. Conclusion

In conclusion, we demonstrate that nonresonant excitation of nearly defect-free semiconductor nanowires is followed by bimolecular interconversion of the initially generated free electron–hole plasma into an exciton population. An increase in excitation fluence leads to faster initial exciton formation, while at long times and low charge-pair densities a reduction of the exciton formation rate presents an obstacle to the system attaining thermal equilibrium. Analysis of the emission lineshape showed that the conducting-to-insulating transition

occurs gradually over total electron–hole charge pair density of  $2\text{--}4 \times 10^{16} \text{ cm}^{-3}$ . We attribute the smoothness of this Mott transition to the slow carrier cooling during the bimolecular interconversion of free charge carriers into excitons and the presence of chemical-potential fluctuations. For “bare” GaAs core NWs for which the passivating shell layer was absent we found that both free-charge and exciton dynamics are dominated by rapid trapping at defect sites within a few picoseconds after excitation and thus a clear Mott transition cannot be observed. For nanowires the surface-to-volume ratio is inherently high, which results in optoelectronic properties highly sensitive to surface defect states. Our results therefore demonstrate that high-quality nanowires are model systems for investigating fundamental scientific effects in 1D heterostructures.

## 4. Experimental Section

**Growth of GaAs Core–Shell–Skin Nanowires:** GaAs core–shell–skin (CSS) NWs were grown on semi-insulating GaAs(111) B substrates with a 50-nm gold-colloid seeded vapor-liquid-solid metal-organic chemical vapor deposition technique. Trimethylgallium and  $\text{AsH}_3$  were used as precursors. The NWs were grown via a two-temperature growth procedure to minimize the formation of twin-defects.<sup>[26]</sup> The growth was initiated with a nucleation step at high temperature ( $450 \text{ }^\circ\text{C}$ ) and rapidly ramped down to the subsequent growth temperature ( $375 \text{ }^\circ\text{C}$ ). We have previously shown that the coaxial overgrowth of 30 nm AlGaAs/ 5 nm GaAs shell–skin layers onto the surface of the GaAs NW cores is essential to reduce the surface defect density and to prevent the oxidation of the AlGaAs layers.<sup>[14]</sup> The AlGaAs shell layer was grown at higher temperature ( $650 \text{ }^\circ\text{C}$ ) to obtain compositional and structural uniformity, as confirmed in a representative SEM image shown in Figure 1a. Full details of the growth procedure have been previously reported.<sup>[14,26]</sup> To eliminate the otherwise dominant photoluminescence signal from the GaAs substrate, the NWs were then transferred from the as-grown substrate to a z-cut quartz substrate by gently touching the two substrates together.

**Time-Integrated and Time-Resolved Photoluminescence Measurements:** For time-integrated and time-resolved photoluminescence (PL) measurements, the sample was maintained at a temperature of 10 K in a liquid-helium flow cryostat. Time-resolved PL measurements were performed using a PL up-conversion set-up that has already been described in detail elsewhere.<sup>[27]</sup> The sample was excited at a photon energy of 1.68 eV with the output from a mode-locked Ti:Sapphire laser oscillator supplying 100-fs pulses at 82 MHz repetition rate. The PL was gated optically in a  $\beta$ -barium borate crystal using a split-off part of the laser output that was subjected to an adjustable time delay with respect to the excitation pulse. Time-resolved and time-integrated PL spectra were recorded with a liquid-nitrogen cooled charge-coupled device (CCD) detector connected to a spectrometer, and corrected for the spectral response of the apparatus. The spectral resolution of the time-resolved and time-integrated PL systems at the selected detection wavelengths was 32 and 4 meV, respectively, and the former system had a time-resolution of 200 fs.

## Supporting Information

Supporting Information is available from the Wiley Online Library or from the author.

## Acknowledgements

The authors thank the Engineering and Physical Sciences Research Council, the Australian Research Council and the Australian National Fabrication Facility for financial support. C.-K.Y. gratefully acknowledges support through a Merdeka Scholarship.

- [1] I. Gur, N. A. Fromer, M. L. Geier, A. P. Alivisatos, *Science* **2005**, *310*, 462.
- [2] J. Hahm, C. M. Lieber, *Nano Lett.* **2004**, *4*, 51.
- [3] M. C. McAlpine, R. S. Friedman, S. Jin, K. H. Lin, W. U. Wang, C. M. Lieber, *Nano Lett.* **2003**, *3*, 1531.
- [4] R. P. Prasankumar, P. C. Upadhyaya, A. Taylor, *J. Phys. Status Solidi B* **2009**, *246*, 1973.
- [5] J. Puthussery, A. D. Lan, T. H. Kosel, M. Kuno, *ACS Nano* **2008**, *2*, 357.
- [6] J. F. Wang, M. S. Gudiksen, X. F. Duan, Y. Cui, C. M. Lieber, *Science* **2001**, *293*, 1455.
- [7] R. Kumar, A. S. Vengurlekar, A. V. Gopal, T. Melin, F. Laruelle, B. Etienne, J. Shah, *Phys. Rev. Lett.* **1998**, *81*, 2578.
- [8] L. V. Titova, T. B. Hoang, J. M. Yarrison-Rice, H. E. Jackson, Y. Kim, H. J. Joyce, Q. Gao, H. H. Tan, C. Jagadish, X. Zhang, J. Zou, L. M. Smith, *Nano Lett.* **2007**, *7*, 3383.
- [9] L. K. van Vugt, S. J. Veen, E. Bakkers, A. L. Roest, D. Vanmaekelbergh, *J. Am. Chem. Soc.* **2005**, *127*, 12357.
- [10] O. Demichel, V. Calvo, A. Besson, P. Noe, B. Salem, N. Pauc, F. Oehler, P. Gentile, N. Magnea, *Nano Lett.* **2010**, *10*, 2323.
- [11] P. U. Jepsen, W. Schairer, I. H. Libon, U. Lemmer, N. E. Hecker, M. Birkholz, K. Lips, M. Schall, *Appl. Phys. Lett.* **2001**, *79*, 1291.
- [12] G. Kalyuzhny, R. W. Murray, *J. Phys. Chem. B* **2005**, *109*, 7012.
- [13] P. Parkinson, J. Lloyd-Hughes, Q. Gao, H. H. Tan, C. Jagadish, M. B. Johnston, L. M. Herz, *Nano Lett.* **2007**, *7*, 2162–2165.
- [14] P. Parkinson, H. J. Joyce, Q. Gao, H. H. Tan, X. Zhang, J. Zou, C. Jagadish, L. M. Herz, M. B. Johnston, *Nano Lett.* **2009**, *9*, 3349.
- [15] L. V. Titova, T. B. Hoang, H. E. Jackson, L. M. Smith, J. M. Yarrison-Rice, Y. Kim, H. J. Joyce, H. H. Tan, C. Jagadish, *Appl. Phys. Lett.* **2006**, *89*, 173126.
- [16] S. Schmitt-Rink, D. S. Chemla, D. A. B. Miller, *Phys. Rev. B* **1985**, *32*, 6601.
- [17] D. S. Chemla, D. A. B. Miller, *J. Opt. Soc. Am. B* **1985**, *2*, 1155.
- [18] N. Peyghambarian, H. M. Gibbs, J. L. Jewell, A. Antonetti, A. Migus, D. Hulin, A. Mysyrowicz, *Phys. Rev. Lett.* **1984**, *53*, 2433.
- [19] A. H. Simon, S. J. Kirch, J. P. Wolfe, *Phys. Rev. B* **1992**, *46*, 10098.
- [20] C. Klingshirn, *Semiconductor Optics*; Springer-Verlag, Berlin, **1997**.
- [21] J. Shah, M. Combescot, A. H. Dayem, *Phys. Rev. Lett.* **1977**, *38*, 1497.
- [22] N. F. Mott, *Proc. Phys. Soc. London* **1949**, *62*, 416.
- [23] H. Schweizer, A. Forchel, A. Hangleiter, S. Schmittrink, J. P. Lowenau, H. Haug, *Phys. Rev. Lett.* **1983**, *51*, 698.
- [24] H. W. Yoon, M. D. Sturge, L. N. Pfeiffer, *Solid State Commun.* **1997**, *104*, 287.
- [25] L. Kappei, J. Szczytko, F. Morier-Genoud, B. Deveaud, *Phys. Rev. Lett.* **2005**, *94*, 147403.
- [26] H. J. Joyce, Q. Gao, H. H. Tan, C. Jagadish, Y. Kim, X. Zhang, Y. N. Guo, J. Zou, *Nano Lett.* **2007**, *7*, 921.
- [27] M. H. Chang, F. J. M. Hoeben, P. Jonkheijm, A. P. H. J. Schenning, E. W. Meijer, C. Silva, L. M. Herz, *Chem. Phys. Lett.* **2006**, *418*, 196.
- [28] C. Piermarocchi, F. Tassone, V. Savona, A. Quattropani, P. Schwendimann, *Phys. Rev. B* **1997**, *55*, 1333.
- [29] T. C. Damen, J. Shah, D. Y. Oberli, D. S. Chemla, J. E. Cunningham, J. M. Kuo, *Phys. Rev. B* **1990**, *42*, 7434.
- [30] I. Robel, R. Gresback, U. Kortshagen, R. D. Schaller, V. I. Klimov, *Phys. Rev. Lett.* **2009**, *102*, 177404.
- [31] U. Strauss, W. W. Ruhle, K. Kohler, *Appl. Phys. Lett.* **1993**, *62*, 55.
- [32] J. Szczytko, L. Kappei, J. Berney, F. Morier-Genoud, M. T. Portella-Oberli, B. Deveaud, *Phys. Rev. Lett.* **2004**, *93*, 137401.
- [33] G. Rupper, N. H. Kwong, R. Binder, *Phys. Rev. Lett.* **2006**, *97*, 117401.
- [34] D. Robart, X. Marie, B. Baylac, T. Amand, M. Brousseau, G. Bacquet, G. Debart, R. Planel, J. M. Gerard, *Solid State Commun.* **1995**, *95*, 287.
- [35] R. T. Phillips, G. C. Nixon, T. Fujita, M. Y. Simmons, D. A. Ritchie, *Solid State Commun.* **1996**, *98*, 287.
- [36] D. L. Smith, D. S. Pan, T. C. McGill, *Phys. Rev. B* **1975**, *12*, 4360.
- [37] R. Ulbrich, *Phys. Rev. B* **1973**, *8*, 5719.
- [38] P. Vashishta, R. K. Kalia, *Phys. Rev. B* **1982**, *25*, 6492.
- [39] G. Trankle, H. Leier, A. Forchel, H. Haug, C. Ell, G. Weimann, *Phys. Rev. Lett.* **1987**, *58*, 419.
- [40] A. Chomette, B. Deveaud, A. Regreny, G. Bastard, *Phys. Rev. Lett.* **1986**, *57*, 1464.
- [41] N. J. Borys, M. J. Walter, J. Huang, D. V. Talapin, J. M. Lupton, *Science* **2010**, *330*, 1371.

Received: January 23, 2012  
 Published online: